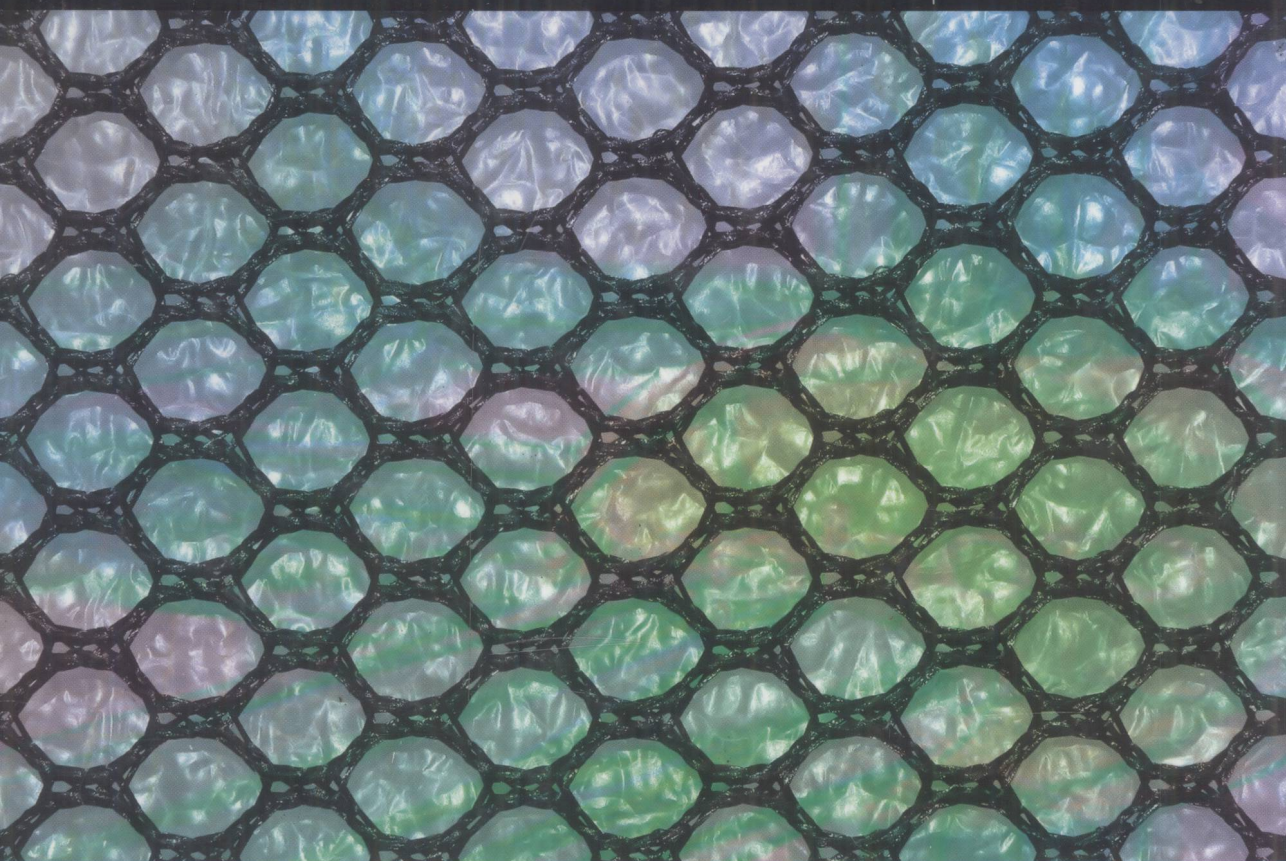




ENGINEERING IN MEDICINE & BIOLOGY

Hedi Mattoussi • Jinwoo Cheon | editors



# Inorganic Nanoprobes

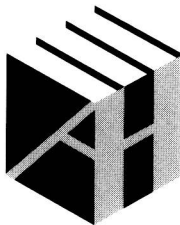
FOR BIOLOGICAL SENSING AND IMAGING

R318  
I58

# Inorganic Nanoprobes for Biological Sensing and Imaging

Hedi Mattoussi  
Jinwoo Cheon

*Editors*



**ARTECH  
HOUSE**

BOSTON | LONDON  
artechhouse.com



E2009003807

**Library of Congress Cataloging-in-Publication Data**

A catalog record for this book is available from the U. S. Library of Congress.

**British Library Cataloguing in Publication Data**

A catalogue record for this book is available from the British Library.

ISBN-13: 978-1-59693-196-1

**Cover design by Igor Valdman**

© 2009 ARTECH HOUSE, INC.

685 Canton Street

Norwood, MA 02062

All rights reserved. Printed and bound in the United States of America. No part of this book may be reproduced or utilized in any form or by any means, electronic or mechanical, including photocopying, recording, or by any information storage and retrieval system, without permission in writing from the publisher.

All terms mentioned in this book that are known to be trademarks or service marks have been appropriately capitalized. Artech House cannot attest to the accuracy of this information. Use of a term in this book should not be regarded as affecting the validity of any trademark or service mark.

10 9 8 7 6 5 4 3 2 1

# **Inorganic Nanoprobes for Biological Sensing and Imaging**



## Artech House Series Engineering in Medicine & Biology

Series Editors

Martin L. Yarmush, Harvard Medical School  
Christopher J. James, University of Southampton

*Advanced Methods and Tools for ECG Data Analysis*,  
Gari D. Clifford, Francisco Azuaje, and Patrick E. McSharry, editors

*Advances in Photodynamic Therapy: Basic, Translational, and Clinical*,  
Michael Hamblin and Pawel Mroz, editors

*Biological Database Modeling*, Jake Chen and Amandeep S. Sidhu, editors

*Biomedical Informatics in Translational Research*, Hai Hu, Michael Liebman,  
and Richard Mural

*Biomedical Surfaces*, Jeremy Ramsden

*Genome Sequencing Technology and Algorithms*, Sun Kim, Haixu Tang, and  
Elaine R. Mardis, editors

*Inorganic Nanoprobes for Biological Sensing and Imaging*, Hedi Mattoussi  
and Jinwoo Cheon, editors

*Intelligent Systems Modeling and Decision Support in Bioengineering*,  
Mahdi Mahfouf

*Life Science Automation Fundamentals and Applications*, Mingjun Zhang,  
Bradley Nelson, and Robin Felder, editors

*Microscopic Image Analysis for Life Science Applications*, Jens Rittscher,  
Stephen T. C. Wong, and Raghu Machiraju, editors

*Next Generation Artificial Vision : Reverse Engineering the Human Visual  
System*, Maria Petrou and Anil Bharath, editors

*Systems Bioinformatics: An Engineering Case-Based Approach*, Gil Alterovitz  
and Marco F. Ramoni, editors

*Systems Engineering Approach to Medical Automation*, Robin Felder.

*Translational Approaches in Tissue Engineering and Regenerative Medicine*,  
Jeremy Mao, Gordana Vunjak-Novakovic, Antonios G. Mikos, and  
Anthony Atala, editors

# Contents

## CHAPTER 1

Colloidal Quantum Dots: Synthesis, Photophysical Properties, and Biofunctionalization Strategies	1
1.1 Introduction	1
1.2 Chemistry and Physics of Semiconductor Quantum Dots	2
1.2.1 Basic Physical Properties of Semiconductor Quantum Dots	2
1.2.2 Synthesis, Characterization, and Capping Strategies	4
1.3 Strategies for Surface-Functionalization and Conjugation to Biomolecules	13
1.3.1 Water-Solubilization Strategies	13
1.3.2 Methods for Conjugating QDs with Biomolecular Receptors	18
1.4 Concluding Remarks and Future Outlook	19
Acknowledgments	20
References	21

## CHAPTER 2

Colloidal Chemical Synthesis of Organic-Dispersible Uniform Magnetic Nanoparticles	27
2.1 Magnetism of Nanoparticles	27
2.2 Transition Metal Nanoparticles	30
2.2.1 Cobalt Nanoparticles	30
2.2.2 Iron and Nickel Nanoparticles	32
2.3 Metal Alloy Nanoparticles	33
2.3.1 FePt Nanoparticles	33
2.3.2 Other Metal Alloy Nanoparticles	34
2.4 Metal Oxide Nanoparticles	35
2.4.1 Monometallic Oxide Nanoparticles	35
2.4.2 Bimetallic Ferrite Nanoparticles	38
2.5 Representative Synthetic Procedures for Magnetic Nanoparticles	39
2.5.1 Iron Nanoparticles	39
2.5.2 Iron Oxide Nanoparticles	40
References	41

## CHAPTER 3

Peptide-Functionalized Quantum Dots for Live Diagnostic Imaging and Therapeutic Applications	45
3.1 Introduction	45

3.2	Phytochelatin Peptides: The All-in-One Solubilization/ Functionalization Approach	47
3.3	Colloidal and Photophysical Properties of Peptide-Coated Qdots	50
3.4	Live Cell Dynamic Imaging	52
3.4.1	Single-Particle Tracking of Cell-Surface Membrane Receptors	52
3.4.2	Peptide-Mediated Intracellular Delivery and Targeting of Qdots	54
3.5	Live Animal Imaging	55
3.5.1	Near-Infrared Deep-Tissue Dual-Modality Imaging	56
3.5.2	In Vivo Targeting of Tumor Vasculature	57
3.6	Beyond Diagnostic Imaging: Sensing and Therapeutic Applications	59
3.6.1	Cleavable Peptides for Proteases Activity	59
3.6.2	Photodynamic Therapy	61
3.7	Conclusion and Perspectives	63
	Acknowledgments	64
	References	64

## CHAPTER 4

	Resonance Energy Transfer-Based Sensing Using Quantum Dot Bioconjugates	71
4.1	Introduction and Background	71
4.2	Unique Attributes of Quantum Dots As FRET Donors	73
4.2.1	Improving the Spectral Overlap by Tuning QD Emission	73
4.2.2	Significant Reduction of Direct Excitation of the Acceptor	74
4.2.3	Increase FRET Efficiency by Arraying Multiple Acceptors around a Single QD	74
4.2.4	Achieving Multiplex FRET Configurations with One Excitation Source	76
4.2.5	Multiphoton FRET Configurations	77
4.3	FRET-Based Biosensing with Quantum Dots	79
4.3.1	Competitive Sensing Using QD-Protein Conjugates	79
4.3.2	Sensing Enzymatic Activity Using QD-Peptide and QD-Oligonucleotide Substrates	82
4.3.3	Detection of Hybridization Using QD-Nucleic Acid Conjugates	85
4.3.4	pH and Ion Sensing	88
4.4	Quantum Dots As Sensitizers for Photodynamic Therapy	91
4.5	Special Sensing Configurations	93
4.6	Conclusions and Outlook	96
	Acknowledgments	97
	References	97

## CHAPTER 5

	Use of Luminescent Quantum Dots to Image and Initiate Biological Functions	101
5.1	Introduction	101
5.2	Multivalency Allows Multifunctionality	103
5.3	Stimuli-Responsive Polymers and Qds As Tools for Imaging	109
5.4	Conclusions	110
	Acknowledgments	111

References	111
<b>CHAPTER 6</b>	
Single Particle Investigation of Biological Processes Using QD-Bioconjugates	115
6.1 Introduction	115
6.2 Physical Properties of Single QDs	116
6.3 In Vitro Detection of Biomolecular Interactions Using Single QD Fluorescence	116
6.3.1 Detection of Biomolecules Using Multicolor Colocalization of QD Probes	117
6.3.2 Colocalization Studies Using Streptavidin-Coupled QD-Dye Pairs	119
6.3.3 Fluorescence Energy Transfer from Single QD to Organic Fluorophores	119
6.4 In Vitro and In Vivo Tracking of Protein Using Single QDs	124
6.4.1 In Vitro Detection of Kinesin and Myosin Motor Movement	124
6.4.2 Tracking of Protein Receptors in Live Cells	126
6.5 Conclusion	129
Acknowledgments	129
References	130
<b>CHAPTER 7</b>	
Assessment of the Issues Related to the Toxicity of Quantum Dots	133
7.1 Introduction	133
7.2 General Considerations	134
7.2.1 Routes of Exposure	134
7.2.2 Mechanisms of Cellular Internalization of QDs	135
7.2.3 Detection of QD-Induced Cytotoxicity	136
7.3 Mechanisms of Quantum Dots Cytotoxicity	138
7.3.1 Release of Toxic Metal Ions	138
7.3.2 Effects of Capping Materials on Cytotoxicity	140
7.3.3 Effects of QD Size on Cytotoxicity	141
7.3.4 Effects of Reactive Oxygen Species on Cytotoxicity	142
7.3.5 Effects of QDs on Genomic DNA	147
7.4 Bioaccumulation and Clearance of QDs	150
7.5 Outlook	153
Acknowledgments	154
References	154
<b>CHAPTER 8</b>	
Chemical and Biological Sensing Based on Gold Nanoparticles	161
8.1 Introduction	161
8.2 Synthesis of Gold Nanoparticles	162
8.3 Physical Properties of Gold Nanoparticles	164
8.4 Colorimetric Sensing	165
8.4.1 Colorimetric Detection of Metal Ions and Anions	166

8.4.2	Colorimetric Detection of Biomaterials	167
8.5	Fluorescence Sensing	170
8.6	Electrical and Electrochemical Sensing	172
8.7	Surface Enhanced Raman Scattering-Based Sensing	179
8.8	Gold Nanoparticle-Amplified SPR Sensing	180
8.9	Quartz Crystal Microbalance-Based Sensing	181
8.10	Gold Nanoparticle-Based Bio-Barcode Assay	182
8.11	Concluding Remarks	183
	Acknowledgments	185
	References	185

## **CHAPTER 9**

	Plasmon-Resonant Gold Nanorods: Photophysical Properties Applied Toward Biological Imaging and Therapy	197
9.1	Introduction	197
9.2	Synthesis	198
9.3	Optical Properties	200
9.3.1	Absorption	200
9.3.2	Plasmon-Resonant Scattering	202
9.3.3	Linear Photoluminescence	202
9.3.4	Nonlinear Optical Properties	203
9.3.5	Other Optical Properties	205
9.4	Surface Chemistry and Biocompatibility	206
9.4.1	Bioconjugation Methods	206
9.4.2	Cytotoxicity and Nonspecific Cell Uptake	208
9.5	Biological Applications of Gold Nanorods	209
9.5.1	Contrast Agents for Imaging	209
9.5.2	Photothermal Therapy	213
9.5.3	Ex Vivo Bioanalytical Applications	215
9.6	Outlook	217
	References	218

## **CHAPTER 10**

	Magnetic Nanoparticles in Biomedical Applications	235
10.1	Introduction	235
10.2	Nanoscale Magnetic Properties	235
10.3	Magnetic Resonance Imaging (MRI) Contrast Agent	237
10.4	Magnetic Separation	241
10.5	Magnetic Drug Delivery	245
10.6	Conclusions	247
	References	247

## **CHAPTER 11**

	Magnetic Nanoparticles-Assisted Cellular MR Imaging and Their Biomedical Applications	251
11.1	Introduction	251



11.2	Characterization of MRI Contrast Agents or Magnetic Nanoparticles Used in Cell Labeling for CMRI	252
11.2.1	Paramagnetic Agents	252
11.2.2	Superparamagnetic Agents	253
11.3	Methods for Labeling Cells with Magnetic Nanoparticles for CMRI	256
11.3.1	Endocytosis of Contrast Agents	256
11.3.2	Modified Nanoparticles for Cell Labeling	257
11.3.3	Transfection Agent Mediated Cell Labeling	260
11.3.4	Other Methods of Cell Labeling	260
11.4	Methods to Monitor the Functional Status of Labeled Cells or Toxicity Following Labeling	261
11.4.1	Determination of Cell Viability	262
11.4.2	Determination of Cell Function	263
11.4.3	Determination of Cell Differentiation Capacity	263
11.5	MRI Techniques to Detect Cells Labeled with Superparamagnetic Iron Oxides	263
11.6	Animal Studies That Have Utilized CMRI	265
11.6.1	Stem Cell Tracking	265
11.6.2	Intracranial Tumor Studies	265
11.6.3	Tumor Angiogenesis	266
11.6.4	Stroke and Trauma Models	268
11.6.5	Myocardial Infarction and Vascular Models	269
11.6.6	Models of Multiple Sclerosis	272
11.7	Translation to the Clinic	273
11.7.1	Human Studies	273
11.7.2	Regulatory Issues	274
	References	276
	About the Editors	289
	List of Contributors	290
	Index	293

# Colloidal Quantum Dots: Synthesis, Photophysical Properties, and Biofunctionalization Strategies

Kimihiro Susumu, Igor L. Medintz, and Hedi Mattoussi

## 1.1 Introduction

Fluorescence tagging of biological molecules is a commonly used approach in biotechnology that has relied on conventional organic fluorophores and fluorescent proteins [1–3]. All available organic fluorophores and fluorescent proteins, however, have some inherent limitations that reduce their effective use to develop biological sensing and imaging. Among these, the most limiting properties are narrow excitation spectral windows, broad photoluminescence (PL) spectra, and low resistance to chemical and photo-degradation [4, 5]. Luminescent semiconductor nanocrystals—often referred to as quantum dots (QDs), such as those made of CdSe and PbSe cores—in comparison offer several unique properties and promise significant advantages in certain bioanalytical and imaging applications [4–8]. Because they have broad absorption envelopes, extending from the ultraviolet (UV) to the band edge, it is possible to simultaneously excite QDs of different emission colors at a single wavelength, making them suitable for multiplexing applications. This promising feature is very difficult to achieve with conventional organic fluorophores. Depending on the materials used, QDs can emit light over a wide range of wavelengths from the visible to near infrared (NIR) regions of the optical spectrum [4, 5, 9–15]. Since the first reports on the use of QD in biology were published, there have been several demonstrations showing that QDs conjugated with biomolecular receptors (including peptides, proteins, and DNA) can be used in a range of biological applications, such as sensing, imaging, and diagnostics. However, successful integration of QDs in biotechnology necessitates a thorough understanding of the nanocrystals, namely their reproducible synthetic routes, surface treatment/functionalization, and biocompatibility.

In this chapter, we provide an overview of the most commonly used synthetic schemes to make colloidal nanocrystals, along with their photophysical and structural characterization. We will then describe some of the most effective schemes reported to date to promote water solubility of these nanocrystals and discuss the simplest conjugation techniques that can be reproducibly applied to colloidal QDs.

## 1.2 Chemistry and Physics of Semiconductor Quantum Dots

### 1.2.1 Basic Physical Properties of Semiconductor Quantum Dots

Semiconductor nanocrystals (or QDs) are small crystalline assemblies of a given material consisting of a few hundred to several thousand atoms. Their sizes range anywhere from  $10\text{\AA}$  to  $1,000\text{\AA}$  in radius; the exact range depends on the constituent elements used to make the nanocrystals. They can be divided into two main subgroups: (a) Self-assembled QDs are usually grown in vacuum via molecular beam epitaxy or other lithography techniques; these tend to be anisotropic in shape, “pancake like,” and overall larger at least within the 2-D plane (see Figure 1.1) [10, 16]. (b) Solution grown nanocrystals are colloidal in nature, and they can be spherical with a radius of  $10 \sim 200\text{\AA}$ , as well as cubic, rod-like, triangular, and so on (see Figure 1.1) [17]. Their colloidal feature stems from the fact that they are surface-capped with organic ligands that promote their dispersion in the solution environment.

These nanoscale assemblies are neither wholly atomic nor bulk semiconductors. Instead, they exhibit novel electronic properties attributed to what is commonly referred to as quantum confinement effects: this is the spatial confinement of intrinsic electron and hole carriers to the physical dimensions of the nanocrystal material rather than to bulk length scales. Because they somewhat combine properties that are both bulk-like and atomic-like, they have often been described as “artificial atoms.” These confinement effects manifest when the nanocrystal size becomes comparable to, or smaller than, the bulk Bohr exciton radius [10, 18, 19]. One of the best-known and -understood confinement effects is the widening of the energy band gap with decrease of nanocrystal size. This manifests itself as a blue shift of the first absorption peak and the photoluminescence maximum with decreasing particle size, along with the appearance of discrete energy states in both the valence and conduction bands (Figure 1.1). However, resolution in the excited state energy levels and separation between the valence and conduction band levels depends on the type of semiconducting materials used.

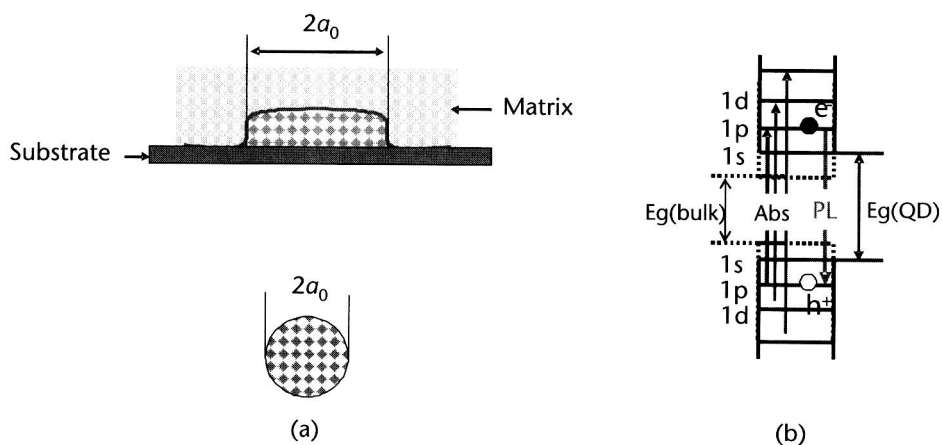


**Figure 1.1** (a) Schematic representation of two QDs, a self-assembled “pancake” nanocrystal (top) and a colloidal nanocrystal (bottom). (b) Representation of the discrete energy levels expected and observed for a nanocrystal, due to quantum confinement effects.

This phenomenon can be understood by a simple extension or adaptation of the expected behavior of a quantum mechanical particle confined in a one-dimensional box of length  $L$  to a three-dimensional box (or sphere) of radius  $a_0$ , where the potential minimum represents the QD and the barrier to escape originates from the abrupt termination of the semiconducting material at the QD surface (boundary conditions) [10, 18, 19]. In this model/description, a carrier is localized within a potential minimum between two infinite barriers. For a one-dimensional box, effects of carrier confinement manifest in quantization of the carrier energies to discrete values that exhibit inverse square dependence on the length of the box ( $E_n \propto n^2/L^2$ , with  $n = 1, 2, 3, \dots$ ).

For a spherical QD with a radius  $a_0$  treated within the conditions of an infinite potential barrier, the electron and hole energy levels in the particle can be written using the following expression:

$$E_{l,n}^{e,b} = \frac{\hbar^2 \beta_{l,n}^2}{2m_{e,b} a_0^2} \quad (1.1)$$

Here  $\beta_{l,n}$  is the  $n$ th root of the spherical Bessel function of order  $l$  (solution obeying the boundary conditions),  $m_{e,b}$  is the effective mass of the electron ( $e$ ) or hole ( $h$ ), and  $a_0$  is the radius of the QD. This treatment predicts discrete (quantized) electron-hole (exciton) transitions, along with an increase in the effective band gap energy (or HOMO-LUMO transition) with decreasing particle size, which can also be expressed as:

$$E_g(\text{QD}) = E_g(\text{bulk}) + \frac{\hbar^2 \pi^2}{2m_{e,b} a_0^2} \quad (1.2)$$

Conversely, (1.1) and (1.2) also predict a decrease in the energy spacing between states with increasing nanocrystal size. It should be noted that the physical behavior of these nanocrystals is also affected by the Coulomb interactions between the confined carriers (these are charged). However, because this contribution/term has a weaker dependence on size (scales as  $1/a_0$  compared to  $\sim 1/a_0^2$  shown in (1.1)), it is small and is often treated as perturbation to the overall energy values. For the interested readers, there are several excellent review articles on the subject published in the past decade, including those recently assembled by Yoffe [16, 19], Gaponenko [18], Efros [10], and Kippeny [20].

Earlier work probing the optical properties of QDs was primarily focused on understanding the correlation between size and spectral shifts in absorption and luminescence based on confinement effects. Today, the absorption properties of CdSe as well as other QDs are relatively well understood with up to 10 excited states in the absorption assigned and theoretical avoided crossings observed [22]. A representative experimental example of absorption spectra for II–VI colloidal QDs is shown in Figure 1.2.

There is a unique spectroscopic property registered primarily for colloidal QDs, but rarely reported for their self-assembled nanocrystal counterparts. Bawendi and coworkers reported in 1996 that under CW laser excitation, the emission of isolated TOP/TOPO-capped single-particle CdSe and CdSe-ZnS QDs was not continuous.

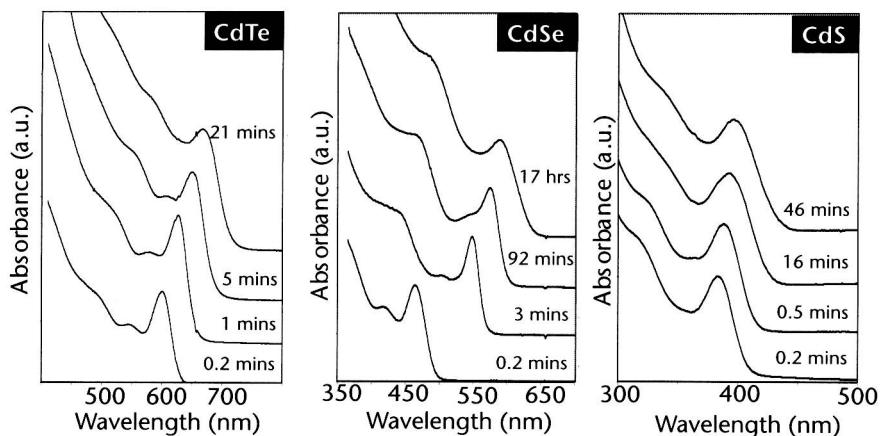


**Figure 1.2** Representative absorption spectra for CdS, CdSe, and CdTe QDs prepared using high-temperature solution reaction. The spectra are shown at successive time intervals of nanocrystal growth. The shift in the position of the first absorption peak reflects an increase in the nanocrystal size. Reproduced from [21], with permission from the American Chemical Society.

Instead, they observed that QDs underwent intermittent on/off photoluminescence, now widely identified as the PL “blinking” of single QDs [23]. Blinking of single QD photoluminescence has since been widely reported in a variety of conditions, including extremely dilute dispersions in polymeric films, surface tethered nanocrystals, and more recently cellular media [24]. In particular, there is a nonvanishing probability for a QD to enter a long dark period. The on/off intermittency in QD emission was attributed to Auger ionization of the QD [23, 25, 26]. Despite the remarkable progress made, this phenomenon is still not fully understood.

## 1.2.2 Synthesis, Characterization, and Capping Strategies

### 1.2.2.1 Growth of Colloidal Nanocrystals in Doped Glasses

A range of experimental techniques such as e-beam lithography, X-ray lithography, molecular beam epitaxy (MBE), ion implantation, and growth in size-restricted environments has been reported for making small nanocrystallites not only of semiconductors but also of metals; colloidal QDs are a subset of those semiconducting nanocrystals. However, the first reported discovery of QDs by Ekimov and Onuschenko used doped silicate glasses [27–34]. The authors showed that if a supersaturated solution of copper and chlorine in glass was heated at high temperatures, controlled precipitation of CuCl within the glass matrix could take place. They further demonstrated that additional heating and annealing of the glass melt systematically creates collections of nano-scale particulates of crystalline CuCl containing a finite number of atoms, ranging from tens to hundreds of angstroms; the authors initially denoted these structures as *quantum droplets*. Following those remarkable demonstrations, growth of QDs made of II–VI semiconductors (e.g., CdS and CdSe) in glass was achieved by doping the melt with salts of the desired materials/precursors [27, 29, 35]. When the temperature of the glass rapidly decreases, small nuclei of the semiconductor are generated. Following heat treat-



ment over temperatures ranging from 400 to 1,000 degrees C, nucleation and growth culminate in the formation of small spherical crystalline particles of semiconductor dispersed in the amorphous glass matrices. This technique provided highly crystalline nanoparticles in glass host samples that can support very large (a few hundred angstroms) QDs. However, because the QDs remain trapped within a solid glass matrix, these nanocrystals cannot be easily manipulated to alter surface chemistry or improve their size distribution.

### 1.2.2.2 Synthetic Routes of Dispersible and Highly Luminescent QDs

Solution-phase growth of semiconductor nanoparticles carried out within inverse micelles was demonstrated shortly after the first realization of carrier confinements in semiconductor crystallites using doped silicate glasses by Ekimov and coworkers [28–31, 36–38]. This “wet chemistry” route allows preparation of functionalized, and thus dispersible, nanocrystals, by essentially exploiting the natural geometrical structures created by water-in-oil mixtures upon adding an amphiphilic surfactant such as sodium dioctyl sulfosuccinate (AOT), cetyltrimethylammonium bromide (CTAB), and tetraoctylammonium bromide (TOAB) (see schematics in Figure 1.3). This route was in fact demonstrated for a variety of other inorganic nanoparticles. In this technique, one can vary the water content of the mixture to control the size of the water droplets (nanoscale reaction pools) suspended in the oil phase. Addition of appropriate metal salts to the solution, which naturally migrate to the water pools, initiates nucleation and growth of colloidal nanocrystals. This technique has a few advantages including the fact that the reactions are carried out at room temperature. Furthermore, it provides one the unique ability to perform postsynthesis processing of these materials from solutions. This approach, however, was not able to provide QDs that have good crystalline structure and high photoluminescence quantum yields necessary for potential transition to technological use.

A major breakthrough took place in 1993, when Bawendi and coworkers showed that high quality nanocrystals of CdSe QDs with crystalline cores, narrow size distribution (~10 percent), and relatively high quantum yields can be prepared using an *organometallic synthesis* based on the “pyrolysis” of metal-organic precursors [9, 39]. This rationale was confirmed shortly thereafter by other groups including Alivistaos and coworkers [40]. This reaction scheme initially employed

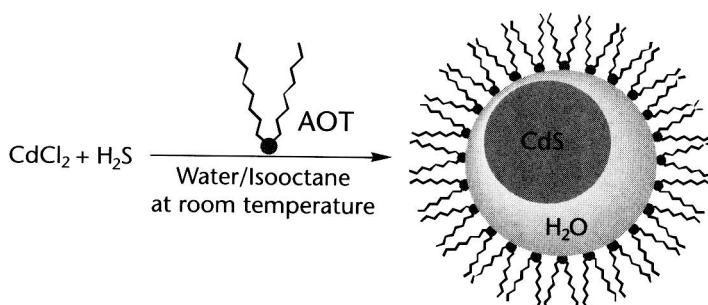


**Figure 1.3** Schematic representation of the growth of CdS semiconductor nanocrystals in inverse micelles. Other materials such as CdSe and CdTe have also been prepared using the inverse micelles approach.

dimethylcadmium ( $\text{CdMe}_2$ ) and trioctylphosphine selenide ( $\text{TOP:Se}$ ), diluted in trioctylphosphine ( $\text{TOP}$ ), and their rapid injection into a hot (280–300 degrees C) coordinating solution of trioctylphosphine oxide ( $\text{TOPO}$ ) (see schematics in Figure 1.4) [39]. They also demonstrated that size distribution can be further improved by postreaction processing. Following this breakthrough, colloidal QDs could be made with quantum yields (QYs) on the order of 5 to 10 percent at room temperature, making fluorescence-based studies of QDs viable and raising the potential for use in technological applications. The QYs of these nanocrystals can reach near unity at low temperature.

Subsequently, Peng and coworkers further refined the reaction scheme and showed that additional precursors that are less volatile and less pyrophoric than  $\text{CdMe}_2$  could effectively be employed to prepare high-quality colloidal nanocrystals [21, 43]. In those studies, they and other groups have eventually outlined the importance of impurities—usually acids coordinating to the metal precursors, such as hexylphosphonic acid (HPA) and tetradecylphosphonic acid (TDPA)—in the reaction progress, and showed that these impurities can be externally controlled. They also applied this rationale to making other types of colloidal nanocrystals, including  $\text{CdTe}$  and  $\text{CdS}$  as well as  $\text{Pb}$ -based QDs. In this route, high purity  $\text{TOPO}$  and controlled amounts of metal coordinating ligands and metal precursors such as  $\text{CdO}$ , cadmium acetate ( $\text{Cd}(\text{OAc})_2$ ), and cadmium acetylacetonate ( $\text{Cd}(\text{acac})_2$ ) were used for preparing  $\text{Cd}$ -based nanocrystals. The high temperature synthetic route was extended to making near-IR emitting QDs by Murray and coworkers (and further confirmed by other groups), using oleic acid and Lead(II) acetate trihydrate or lead oxide for  $\text{PbSe}$  QDs [14, 44, 45]. In most reported methods the selenium precursor still relies on  $\text{TOP:Se}$  [14, 21, 43, 46, 47].

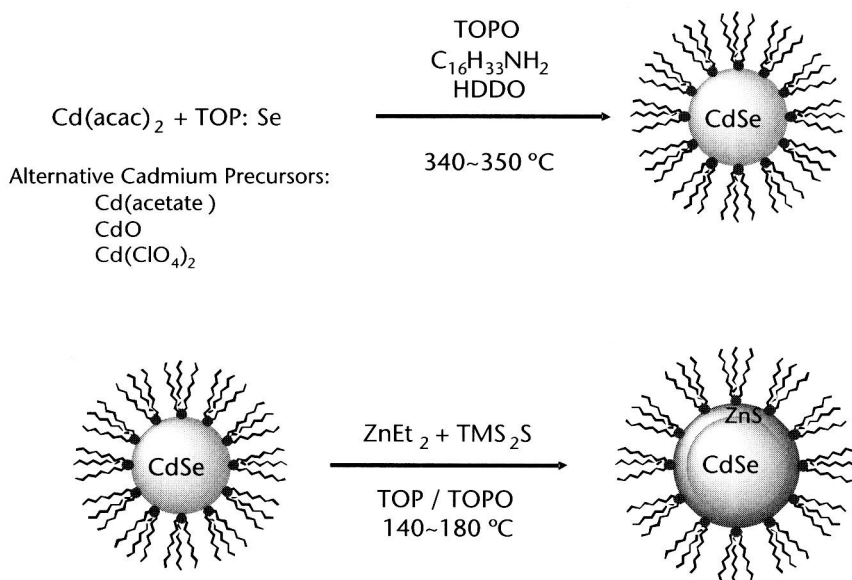


**Figure 1.4** (top) Schematic depiction of the high-temperature organometallic reaction and growth method used for colloidal  $\text{CdSe}$  nanocrystals. (bottom) Reaction scheme for the overcoating  $\text{CdSe}$  quantum dots with  $\text{ZnS}$  using the same high-temperature solution route. Additional details can be found in [41, 42].

In these high-temperature reaction schemes, it has been demonstrated that applying size selective precipitation using polar solvents such as methanol or ethanol following nanocrystal growth could reduce the particle size distribution/polydispersity of the nanocrystals. In addition to reducing polydispersity, this procedure also removes impurities and precipitated metals from the reaction solution [9, 39]. This cleaning step is crucial for nanocrystals made using less reactive precursors and the various metal-coordinating molecules, since larger amounts of unreacted metals, acids, and amines can be left in the final QD crude samples. Available techniques to characterize nanocrystals include high- and low-resolution transmission electron microscopy (TEM), wide angle X-ray diffraction (XRD), small angle X-ray scattering (SAXS), and absorption and fluorescence spectroscopy, which extract information such as size, distribution width, crystal structure, band edge value and emission energy level (see Figures 1.5 and 1.6 and Table 1.1) [9, 11, 21, 39, 41–43, 46–50]. TEM tends to provide slightly smaller values for the inorganic core than SAXS, for example, because TEM does not take into account the amorphous outermost atomic layer on the nanocrystal surface [51].

Additional details on the synthetic routes, structural characterization, physics of quantum confinements effects, and their implications on the electronic and spectroscopic properties of colloidal QDs can be found in these thorough reviews [17, 52]. A summary of the reported synthetic methods for making colloidal QDs is provided in Table 1.2, with particular emphasis on preparations yielding colloidal QDs

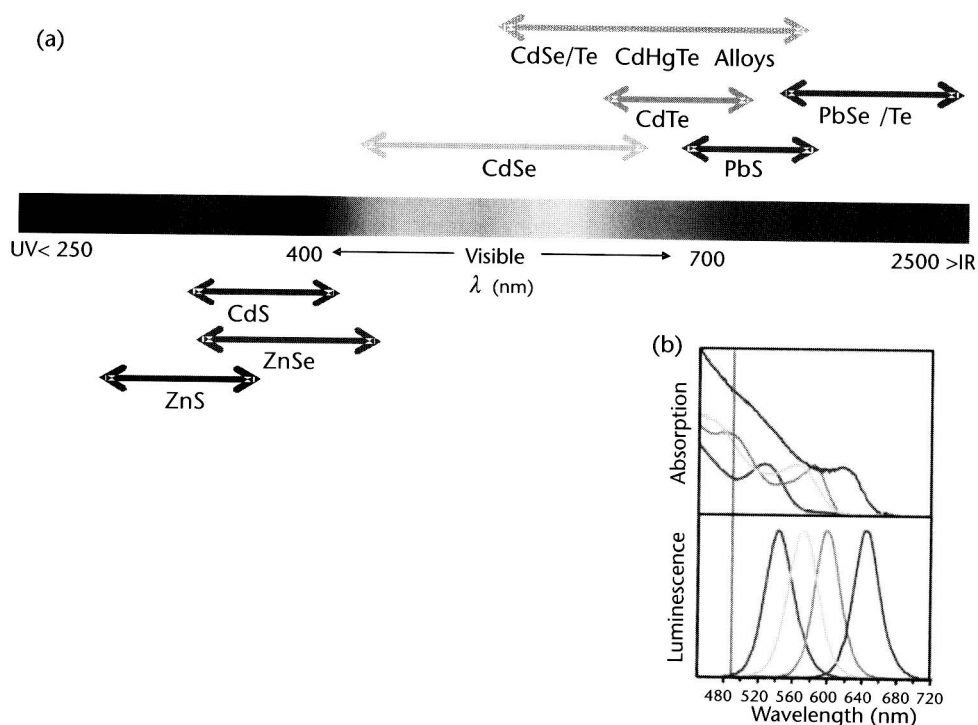


**Figure 1.5** (a) Representative set of emission spectral windows for several types of QD materials. Core materials of II–VI, III–V and hybrid “III–VI” are shown. Partially reproduced from [5], with permission from NPG. (b) A representative example of absorption and normalized emission spectra collected for solutions of CdSe–ZnS QDs. Partially reproduced from [4], with permission from AAS. Other materials not represented here include InP and InAs QDs. (See Color Plate 1.)